SANDIA REPORT

SAND2013-2001
Unlimited Release
March 2013

A Coupled Transport and Solid Mechanics Formulation with Improved Reaction Kinetics Parameters for Modeling Oxidation and Decomposition in a Uranium Hydride Bed

Maher Salloum, Andrew D. Shugard, Michael P. Kanouff, Patricia E. Gharagozloo

Prepared by
Sandia National Laboratories
Albuquerque, New Mexico 87185 and Livermore, California 94550

Sandia National Laboratories is a multi-program laboratory managed and operated by Sandia Corporation, a wholly owned subsidiary of Lockheed Martin Corporation, for the U.S. Department of Energy's National Nuclear Security Administration under contract DE-AC04-94AL85000.

Approved for public release; further dissemination unlimited.

Sandia National Laboratories

Issued by Sandia National Laboratories, operated for the United States Department of Energy by Sandia Corporation.

NOTICE: This report was prepared as an account of work sponsored by an agency of the United States Government. Neither the United States Government, nor any agency thereof, nor any of their employees, nor any of their contractors, subcontractors, or their employees, make any warranty, express or implied, or assume any legal liability or responsibility for the accuracy, completeness, or usefulness of any information, apparatus, product, or process disclosed, or represent that its use would not infringe privately owned rights. Reference herein to any specific commercial product, process, or service by trade name, trademark, manufacturer, or otherwise, does not necessarily constitute or imply its endorsement, recommendation, or favoring by the United States Government, any agency thereof, or any of their contractors or subcontractors. The views and opinions expressed herein do not necessarily state or reflect those of the United States Government, any agency thereof, or any of their contractors.

Printed in the United States of America. This report has been reproduced directly from the best available copy.

Available to DOE and DOE contractors from
U.S. Department of Energy
Office of Scientific and Technical Information
P.O. Box 62
Oak Ridge, TN 37831

Telephone: (865) 576-8401
Facsimile: (865) 576-5728
E-Mail: reports@adonis.osti.gov
Online ordering: http://www.osti.gov/bridge

Available to the public from
U.S. Department of Commerce
National Technical Information Service
5285 Port Royal Rd.
Springfield, VA 22161

Telephone: (800) 553-6847
Facsimile: (703) 605-6900
E-Mail: orders@ntis.fedworld.gov
Online order: http://www.ntis.gov/help/ordermethods.asp?loc=7-4-0#online

SAND2013-2001
Unlimited Release
March 2013

A Coupled Transport and Solid Mechanics Formulation with Improved Reaction Kinetics Parameters for Modeling Oxidation and Decomposition in a Uranium Hydride Bed

Maher Salloum
Andrew D. Shugard
Michael P. Kanouff
Patricia E. Gharagozloo

Sandia National Laboratories
P.O. Box 969
Livermore, California 94551

Abstract

Modeling of reacting flows in porous media has become particularly important with the increased interest in hydrogen solid-storage beds. An advanced type of storage bed has been proposed that utilizes oxidation of uranium hydride to heat and decompose the hydride, releasing the hydrogen. To reduce the cost and time required to develop these systems experimentally, a valid computational model is required that simulates the reaction of uranium hydride and oxygen gas in a hydrogen storage bed using multiphysics finite element modeling. This SAND report discusses the advancements made in FY12 (since our last SAND report SAND2011-6939) to the model developed as a part of an ASC-P&EM project to address the shortcomings of the previous model. The model considers chemical reactions, heat transport, and mass transport within a hydride bed. Previously, the time-varying permeability and porosity were considered uniform. This led to discrepancies between the simulated results and experimental measurements. In this work, the effects of non-uniform changes in permeability and porosity due to phase and thermal expansion are accounted for. These expansions result in mechanical stresses that lead to bed deformation. To describe this, a simplified solid mechanics model for the local variation of permeability and porosity as a function of the local bed deformation is developed. By using this solid mechanics model, the agreement between our reacting bed model and the experimental data is improved. Additionally, more accurate uranium hydride oxidation kinetics parameters are obtained by fitting the experimental results from a pure uranium hydride oxidation measurement to the ones obtained from the coupled transport-solid mechanics model. Finally, the coupled transport-solid mechanics model governing equations and boundary conditions are summarized and recommendations are made for further development of ARIA and other Sandia codes in order for them to sufficiently implement the model.

ACKNOWLEDGMENTS

The authors of this SAND report acknowledge the following people who provided additional assistance to enable the success of the project:

Greg Wagner – *guidance on which portions of the model could not be implemented in the current versions of Sandia codes*

Chris Moen, Paul Spence, Neal Fornaciari, and Mike Chiesa – *program development*

David Robinson – *valuable discussions regarding the experiments*

George Buffleben – *operating the experimental apparatus and conducting most of the experiments*

Scott James – *modeling expertise*

CONTENTS

Acknowledgments 5

Contents 6

Figures 6

Tables 7

1 Introduction 9

2 A Coupled Transport-solid Mechanics Formulation of the oxygen Reactive flow in a uranium hydride bed 11
- 2.1 Solid Mechanics Model Formulation 11
- 2.2 Thermal Conductivity of the Powder Bed 13
- 2.3 Results and Discussion 14
  - 2.3.1 O_2 injection #1 14
  - 2.3.2 O_2 injection #2 16
  - 2.3.3 O_2 injection #3 18

3 Improving the uranium hydride oxidation kinetics parameters 21
- 3.1 Pure Oxidation Experiment (Reactor #4) 21
- 3.2 Fitting the Model to the Experimental Results 24

4 Summary of the governing equations, boundary conditions and numerical methods used to model oxidation and decomposition in a uranium hydride bed 27
- 4.1 Model Geometry and Mesh 27
- 4.2 Governing Equations and Boundary Conditions 29
- 4.3 Coupling Relationships 30
- 4.4 Recommendation for ARIA Developers 32

5 Conclusions 33

6 References 35

7 Distribution 37

FIGURES

Figure 1. A schematic of the axisymmetric reactor model. The schematic shows: (left) the entire model domain, comprised of the O_2 source and flow channels (Ω_1), the UD_3 reactor bed (Ω_2), the frits at the reactor entrance and exit (Ω_3), and the reactor stainless steel housing (Ω_4); and (right) a magnified view of the reactor depicting typical species distribution during the reaction. The temperature is monitored in the experiments at two locations TC#1 and TC#2 at the reactor housing outer surface. 12

Figure 2: Plots of the (a) temperature (^oC), (b) composition, (c) porosity, and (d) permeability (cm^2), inside the bed for O_2 injection #1. The plots are generated during the reaction (t=125 s) and at the end of the injection, as indicated. 15

Figure 3: The measured and predicted (top) pressure decay in the O_2 source vessel, (bottom) temperatures at the locations of thermocouples TC #1 and TC #2, as indicated. The predictions were obtained using the constant permeability model of Kanouff *et.al.* (8) and the current variable permeability model for O_2 injection #1..... 16

Figure 4: Plots of the (a) temperature (^oC), (b) composition, (c) porosity, and (d) permeability (cm^2), inside the bed for O_2 injection #2. The plots are generated during the reaction (t=125 s) and at the end of the injection, as indicated..... 17

Figure 5: The measured and predicted (top) pressure decay in the O_2 source vessel, (bottom) temperatures at the locations of thermocouples TC #1 and TC #2, as indicated. The predictions were obtained using the constant permeability model of Kanouff *et.al.* (8) and the current variable permeability model for O_2 injection #2..... 18

Figure 6: The measured and predicted (top) pressure decay in the O_2 source vessel, (bottom) temperatures at the locations of thermocouples TC #1 and TC #2, as indicated. The predictions were obtained using the constant permeability model of Kanouff *et.al.* (8) and the current variable permeability model for O_2 injection #3..... 20

Figure 7: Experimental apparatus used for all uranium hydride reactor experiments. Reproduced from (8)..... 22

Figure 8: Measured gas pressures during oxygen injection..... 22

Figure 9: Experimentally measured O_2 injection rate..... 23

Figure 10: The measured and predicted temperatures at the locations of thermocouples TC #1 TC #2 and TC #3. The predictions were obtained using current variable permeability model for a pure uranium hydride oxidation scenario using the oxidation kinetic coefficients of Kanouff *et.al.* (9) and the values calibrated with experimental measurements, as indicated. 25

Figure 11: The measured and predicted (top) pressure decay in the O_2 source vessel, (bottom) temperatures at the locations of thermocouples TC #1 and TC #2. The predictions were obtained using current variable permeability model for a pure uranium hydride oxidation scenario using the oxidation kinetic coefficients of Kanouff *et.al.* (9) and the values calibrated with experimental measurements, as indicated..... 26

Figure 12: A schematic of the axisymmetric reactor model. The schematic shows the entire model geometry, comprised of subdomains Ω_1, Ω_2, Ω_3 and Ω_4, and boundaries Γ_1, Γ_2 … Γ_{10}. ... 27

Figure 13: A plot of the recommended mesh inside the bed. The mesh is quadrilateral with a size of 0.1x0.1 mm inside the bed..... 28

TABLES

Table 1: Governing Equations and boundary conditions..... 29

Table 2: Thermophysical properties of the species present in the model..... 30

Table 3: Thermomechanical properties of the solid species present in the model 31

Table 4. Physical properties of the species present in the model..... 31

INTRODUCTION

Uranium hydride powder beds have been used extensively for hydrogen isotope storage (1-3). Uranium hydride is pyrophoric (4-7) and therefore air ingress accidents have been a longstanding concern. Given sufficient air or oxygen, high temperatures can be reached within the bed, leading to hydride decomposition, which produces hydrogen gas. Hydrogen gas release is undesirable in an accident scenario. Alternatively however, injecting oxygen into a uranium hydride bed could be an effective way to quickly generate hydrogen gas for small devices such as portable fuel cells (8). A mathematical model is extremely useful when designing an optimal hydrogen generating reactor. Such a model could also be used to predict the outcome of storage bed air ingress accidents.

A detailed numerical model of the oxidation and decomposition in a uranium hydride bed was developed in the previous years of this project (9). The model explicitly considers rates of chemical reaction, heat transport, and mass transport within the porous bed. The model was developed for comparison to experiments described by Shugard *et al* (8). In the earlier model, it was assumed that a mechanical equilibrium exists within the bed such that the porosity is uniform; and therefore only a function of the mean bed composition over time. The hydraulic permeability is recovered from the mean porosity using Young's law (10); such that it is also uniform within the bed. Comparisons with Shugard *et al.*'s measurements showed this to be a reasonably effective approximation (8). However, discrepancies in the pressure and temperature response of the hydride bed suggest that the permeability computed by this simplified model is not entirely accurate. Furthermore, the oxidation kinetics of uranium hydride are not well quantitatively established in the literature (6-8,11). In the earlier model (9) these kinetics parameters were crudely estimated based on experimental observation of the deuterium-to-oxygen transition rate in the effluent gas and based on the different injection rates used in the experiments (8). Such estimation might not be accurate since discrepancies arose between the experimentally measured and predicted temperature response of the bed.

In this study, different improvements are introduced to the previously developed model. First, the uniform porosity assumption is relaxed by computing a porosity field within the bed. The local permeability is then recovered using Young's law. The thermal and phase expansions occurring in the bed induce deformations that, in turn, result in changes in the local porosity. These deformations are quantified using a solid mechanics model. A simplified linear elastic model is developed to describe bed deformation inside the closed reactor volume. Mass conservation equations are then applied to obtain an expression of the local bed porosity as a function of the spatial deformation. Furthermore, values for the thermal conductivity of the different solid phases present in the bed during the reaction are obtained from the literature. The dependence of the local bed thermal conductivity on the computed local porosity is accounted for, relaxing the constant thermal conductivity assumption used in the previous model.

A new set of uranium hydride oxidation parameters is obtained based on a pure oxidation experiment performed at a very low oxygen injection rate. The kinetics parameters are solved for in terms of Arrhenius type coefficients by minimizing the error between the predicted and measured temperature response of the bed.

The solid mechanics model is coupled to the improved oxidation kinetics transport model. In this report, the extended model is presented, applied to two oxygen injection cases previously simulated (9), and compared to experimental measurements. The model is sought to be implemented in the SIERRA codes at Sandia National Laboratories, mainly in ARIA and ADAGIO. Therefore, we summarize at the end of this report the partial differential equations, the coupling relationships and the boundary conditions involved in the model. We also provide recommendations for the ARIA code developers in order to properly account for the special features encountered in gas reactive flows in porous media.

A COUPLED TRANSPORT-SOLID MECHANICS FORMULATION OF THE OXYGEN REACTIVE FLOW IN A URANIUM HYDRIDE BED

Solid Mechanics Model Formulation

A solid mechanics model based on the reactor geometry described by Shugard *et al.*, (8-9), and depicted in Figure 1 is developed. The reactor is axisymmetric and is divided into four sub-domains: the oxygen (O_2) source and flow channels (Ω_1), the reactor bed (Ω_2), the frits at the reactor entrance and exit (Ω_3), and the reactor stainless steel housing (Ω_4). The model is developed using uranium deuteride (UD_3) since Shugard *et al.*, (8) used UD_3 instead of UH_3 because the resulting deuterium gas is easier to detect.

As O_2 is injected, a reaction front forms leading to the formation of uranium (U) and uranium oxide (U_3O_8), as depicted in Figure 1 (right). The oxidation and decomposition of UD_3 are assumed to be governed by the following chemical reactions:

$$\mathrm{UD_3} + \frac{4}{3}\mathrm{O_2} \rightarrow \frac{1}{3}\mathrm{U_3O_8} + \frac{3}{2}\mathrm{D_2} \quad \text{(Exothermic)}$$

$$\mathrm{UD_3} \rightarrow \mathrm{U} + \frac{3}{2}\mathrm{D_2} \quad \text{(Endothermic)}$$

$$\mathrm{U} + \frac{4}{3}\mathrm{O_2} \rightarrow \frac{1}{3}\mathrm{U_3O_8} \quad \text{(Exothermic)}$$

Additional details about the chemical reactions, model geometry and mathematical formulation can be found in (8, 9).

The consumption and formation of different solid species within the reactor bed induces phase and thermal strain. Because the reactor is closed, these local strains generate stresses, which are transferred to unreacted regions of the bed, causing further deformation. These stresses and deformations are described using a solid mechanics model. The differential equations governing the stresses are assumed to apply only in the reactor bed domain Ω_2. A quasi-static equilibrium is assumed within the bed; and therefore:

$$\nabla \cdot [\sigma] = 0 \tag{1}$$

where $[\sigma]$ is the stress matrix. The boundaries of Ω_2 are assumed to be frictionless, rigid, walls. Assuming linear-elastic and isotropic behavior for the U, UD_3 and U_3O_8 powders, local stress and strain are related by:

$$[\varepsilon^e] = \frac{1+\nu}{E}[\sigma] - \frac{\nu}{E}Tr([\sigma])[\mathrm{I}] \tag{2}$$

where E and ν are the elastic modulus and Poisson's ratio respectively, $[\varepsilon^e]$ is the elastic strain, Tr([σ]) is the trace of [σ], and $[I]$ is the identity matrix. E and ν were obtained from (12-14) for the different phases, as a function of temperature. Assuming the powders behave as linear-elastic solids greatly oversimplifies their behavior, which is better described as elastic-plastic (15). A linear-elastic formulation is selected because it is numerically tractable.

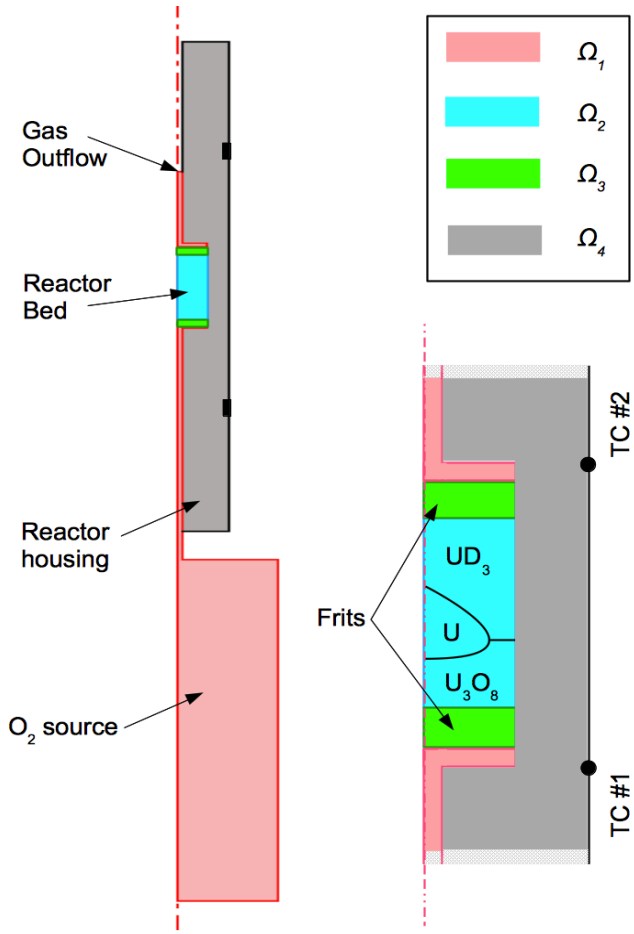

Figure 1. A schematic of the axisymmetric reactor model. The schematic shows: (left) the entire model domain, comprised of the O_2 source and flow channels (Ω_1), the UD_3 reactor bed (Ω_2), the frits at the reactor entrance and exit (Ω_3), and the reactor stainless steel housing (Ω_4); and (right) a magnified view of the reactor depicting typical species distribution during the reaction. The temperature is monitored in the experiments at two locations TC#1 and TC#2 at the reactor housing outer surface.

The total strain is given by the sum of the elastic strain, Eq. 2, and the strain due to the thermal and phase expansions. The total strain $[\varepsilon]$is:

$$[\varepsilon]=[\varepsilon^e]+[\varepsilon^{th}]+[\varepsilon^{ph}] \tag{3}$$

where $[\varepsilon^{ph}]$ and $[\varepsilon^{th}]$ are the strains due thermal and phase expansion respectively. They are:

$$[\varepsilon^{th}] = \alpha \Delta T [I] \tag{4}$$

$$[\varepsilon^{ph}] = \sum_{i=\mathrm{U_3O_8,U}} \frac{\Delta V_i}{3} x_i [I] \tag{5}$$

where α is the thermal expansion coefficient, ΔT is the temperature elevation, ΔV is the phase expansion relative to UD_3 and x is the mole fraction of solid species *i*. Thermal expansion coefficients were obtained from (16-17) for the different species. For U_3O_8 and U, ΔV are 0.536 and -0.432 respectively.

Solving Eqs. 1-5 gives the total strain $[\varepsilon]$. The volumetric expansion e is given by the trace of $[\varepsilon]$:

$$e = Tr([\varepsilon]) \tag{6}$$

The local porosity ϕ is then computed using:

$$\phi = 1 - \frac{(1-\phi_0)\left(1 + \sum_{i=U_3O_8,U} \Delta V_i x_i\right)}{1+e} \tag{7}$$

where ϕ_0=0.605 is the initial (UD_3) bed porosity. In Eq. 7 the (1+e) term accounts for local volumetric expansion or contraction of the porous element; while the $(1-\phi_0)\left(1+\sum_{i=U_3O_8,U} \Delta V_i x_i\right)$ term accounts for phase expansion within the element. Finally, the local bed permeability, κ, is recovered using Young's law (10):

$$\kappa = \frac{\phi d_p^2}{\tau^2}\left(\frac{1}{32} + \frac{5}{12} Kn\right) \tag{8}$$

Thermal Conductivity of the Powder Bed

In addition to the solid mechanics model, improvements to the original transport model (9) are introduced in this study. Previously, the thermal conductivity of the UD_3 bed was considered to be constant all over the bed throughout the simulations. In the current study, the variation of the

thermal conductivity as a function of the bed composition, temperature and porosity is accounted for.

The thermal conductivity of UD_3, U and U_3O_8 are found to be equal to 0.01, 0.01[27+0.0214(T-300)] and 0.000838, respectively (19-21). The porous aspect of the solid materials, however, significantly affects the overall thermal conductivity. When the porosity increases, the distance between solid particles increases where the void space is filled with gas. Thus, the overall thermal conductivity of the porous medium is expected to decrease. Following the analytical study of Nan and Biringer (22), it is assumed that the overall thermal conductivity of species *i* is equal to:

$$k_i = k_{i,solid} \frac{\phi_{0,i}}{\phi} \qquad (9)$$

where ϕ_i is the initial porosity of the species I equal to 0.605, 0.776 and 0.393 for UD_3, U and U_3O_8, respectively and ϕ is the local porosity of the bed calculated by Eq. 7. Thus, the local thermal conductivity inside the reactor bed becomes:

$$\frac{1}{\phi n_{bed}} \sum_{UD_3,U,U_3O_8} k_i \phi_{0,i} [i] \qquad (10)$$

Results and Discussion

The coupled transport-solid mechanics model with the more accurate bed thermal conductivity was used to simulate two O_2 injection experiments, O_2 injection #1 and #2, described in (8). These experiments were carried out successively on a single reactor. In O_2 injection #1, only a small amount of O_2 was injected resulting in partial oxidation of the hydride material. In O_2 injection #2, a larger amount of O_2 was injected into the same reactor, but still leaving about 60% of the hydride material unreacted (8).

O_2 injection #1

During injection #1, 15% of the O_2 required to fully oxidize the bed to U_3O_8 was slowly injected over about 300 seconds. The O_2 was released from a source bottle initially at 20 psia. As the O_2 flows slowly into the bed, the reaction raised the local temperature to about 100 °C; as shown in Figure 2(a). This temperature is low enough that the upstream region of the bed oxidizes directly without noticeable UD_3 decomposition to U, which is apparent in Figure 2(b). The temperature increase and oxidation induce volumetric expansions in the upstream portion of the bed, both of which decrease the local porosity; this is depicted in Figure 2(c, d).

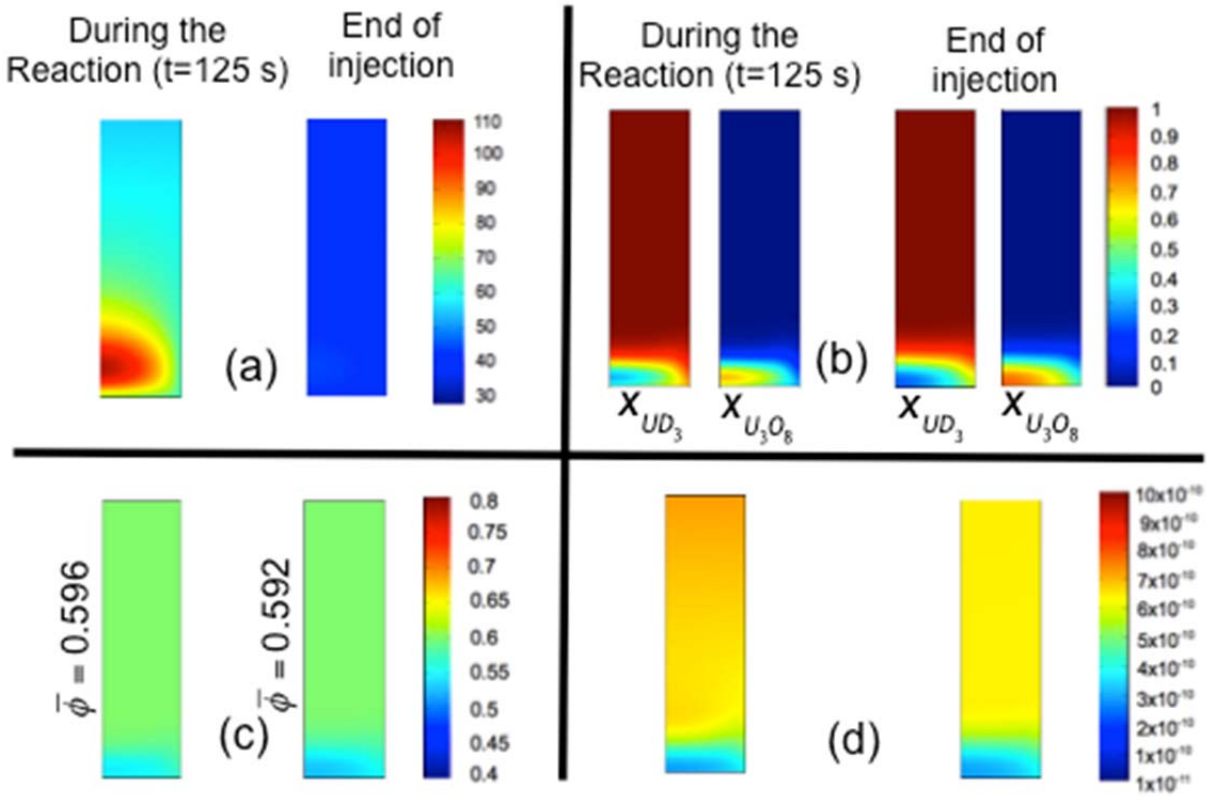

Figure 2: Plots of the (a) temperature (^{o}C), (b) composition, (c) porosity, and (d) permeability (cm^2), inside the bed for O_2 injection #1. The plots are generated during the reaction (t=125 s) and at the end of the injection, as indicated.

The expanding region compresses the unreacted UD_3 powder such that the porosity is decreased on average. This is consistent with the model previous model (8) where it was shown that the uniform porosity decreases as the reaction progresses. The predicted and measured pressure decays in the O_2 source vessel are shown in Figure 3(top). At later times, the bed mechanics model only slightly improves model-and-experiment agreement over the constant permeability model. In Figure 3(bottom) it is apparent that accounting for spatial variations of the permeability has a negligible effect on the reactor temperature response.

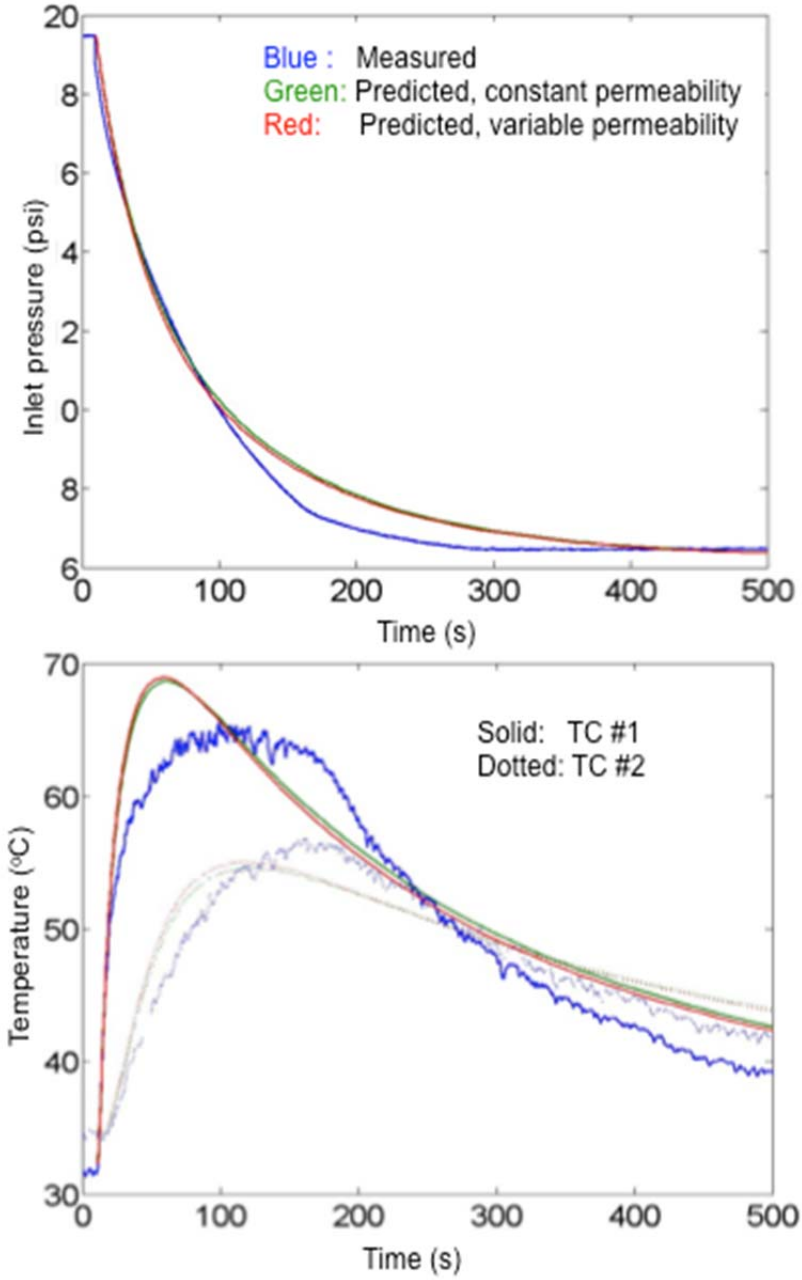

Figure 3: The measured and predicted (top) pressure decay in the O_2 source vessel, (bottom) temperatures at the locations of thermocouples TC #1 and TC #2, as indicated. The predictions were obtained using the constant permeability model of Kanouff *et.al.* (8) and the current variable permeability model for O_2 injection #1.

O_2 injection #2

In this experiment, the O_2 source bottle had a higher initial pressure, 52 psia, and therefore oxygen flowed into the bed more rapidly. Approximately 36% of the bed was oxidized after 500 s. Consequently, heat is generated more rapidly, which leads to higher temperatures (see Figure 4(a)). For much of the injection, local temperatures are high enough to decompose UD_3 and produce U, as shown in Figure 4(b). Thermal and phase expansions are more pronounced in this

case, leading to larger changes in porosity and permeability near the reaction front. It is found that regions downstream of the front experience higher compression stresses, which decrease their porosity and permeability (Figure 4(c, d)). In this case, porosity and permeability in the downstream regions are decreased to about 0.54 and 3×10-10 cm^2 respectively; whereas in O_2 injection #1, they were about 0.59 and 6×10-10 cm^2 respectively. These highly non-uniform porosity and permeability fields significantly impact the pressure and temperature response of the reactor.

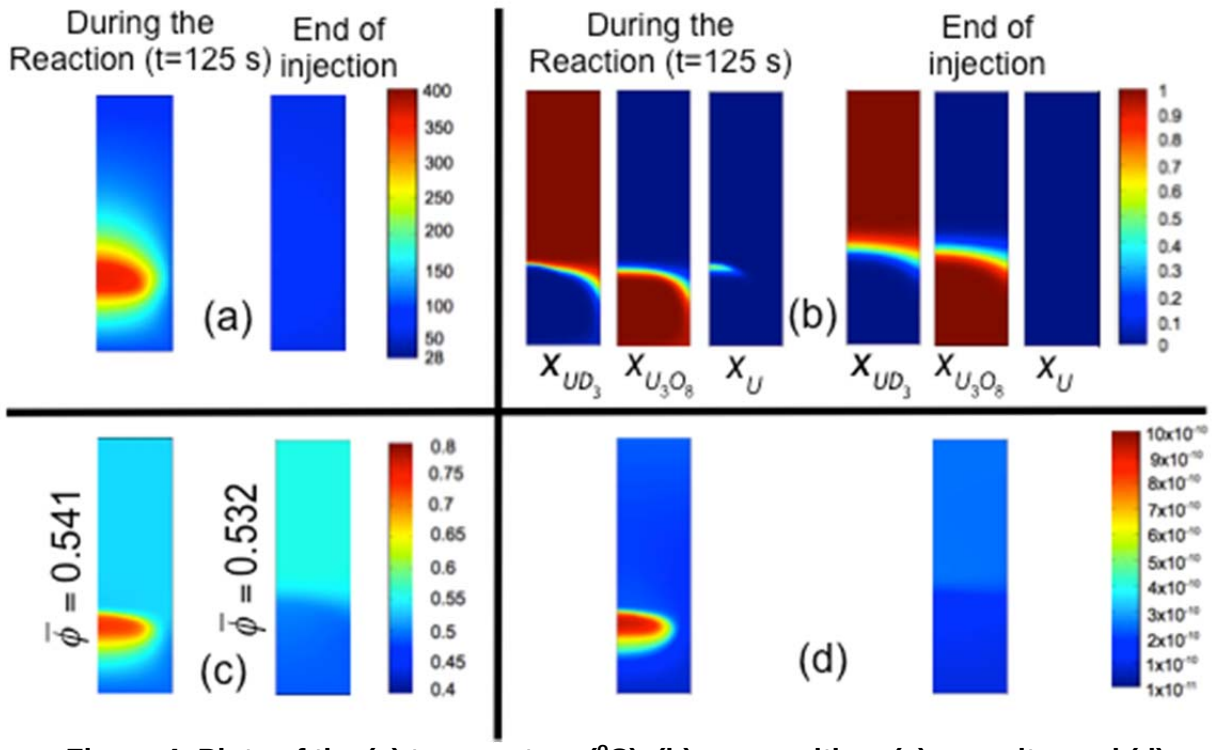

Figure 4: Plots of the (a) temperature (^oC), (b) composition, (c) porosity, and (d) permeability (cm^2), inside the bed for O_2 injection #2. The plots are generated during the reaction (t=125 s) and at the end of the injection, as indicated.

Figure 5 (top) shows the measured O_2 source-volume pressure along with model predictions. It can be seen that including detailed bed mechanics significantly improves the pressure prediction. This is largely because the solid mechanics model more accurately describes the porosity and permeability changes during oxygen injection. Knowledge of the spatially varying permeability gives better knowledge of the overall bed permeability.

Including bed mechanics also improves the temperature prediction. Because the varying oxygen injection rate is captured more accurately, the heat generation rate is more accurately modeled; and therefore the maximum reactor surface temperatures are predicted with greater accuracy. Despite the improvements brought by the solid mechanics model, significant disagreement still exists in the reactor surface temperature response. This may be due to the lack of a truly quantitative model for UD_3 oxidation kinetics. As direct oxidation of uranium hydride has

received very little attention in the literature, kinetic expressions used are described in (8-9) and were determined by crudely fitting these oxygen injection experiments. Additional experiments are needed to validate, and perhaps improve, the UD_3 oxidation rate model.

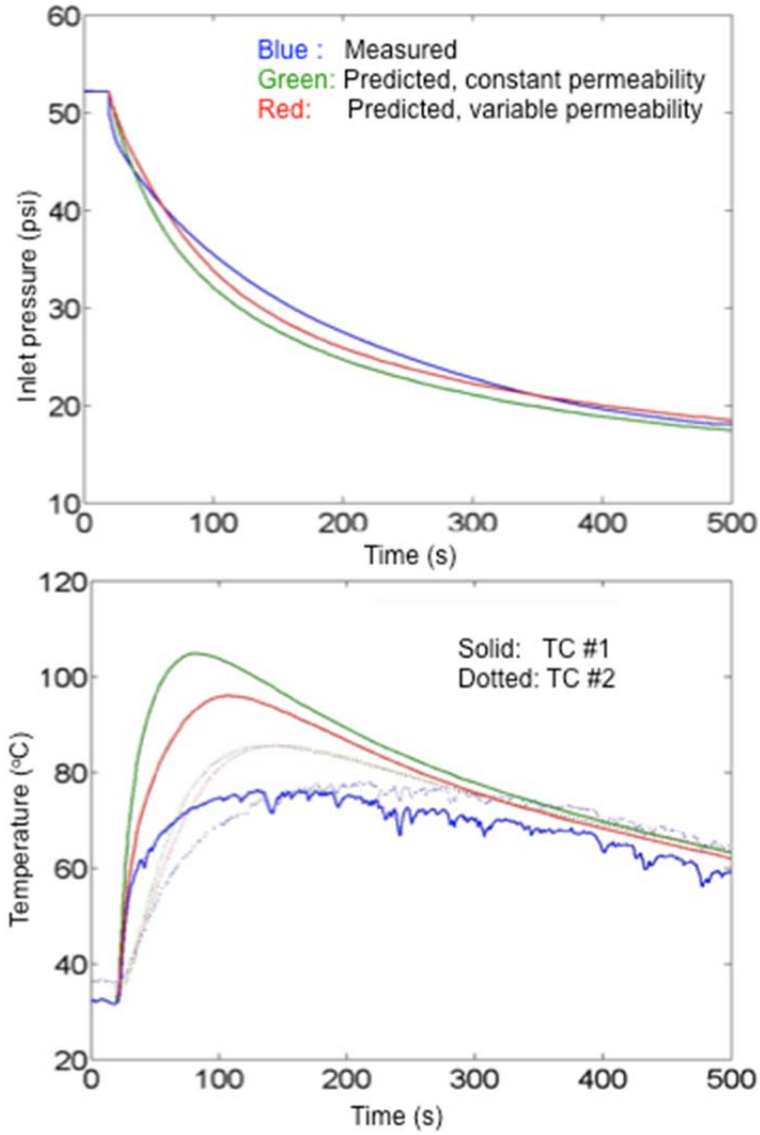

Figure 5: The measured and predicted (top) pressure decay in the O_2 source vessel, (bottom) temperatures at the locations of thermocouples TC #1 and TC #2, as indicated. The predictions were obtained using the constant permeability model of Kanouff *et.al.* (8) and the current variable permeability model for O_2 injection #2.

O_2 injection #3

For this experiment, 150% of the O_2 required to fully oxidize the bed to U_3O_8 was injected over about 500 seconds. The initial state of the reactor for O_2 injection #3 was the final state following O_2 injection #2.

O_2 injection #3 used a larger pressure (171 psia) in the O_2 source vessel than the prior two injection experiments. In addition, the piston-driver (see Figure 7) was used to deliver oxygen at more of a constant pressure. The large source pressure creates larger O_2 flow rates, reaction rates, temperatures, and significantly more UD_3 decomposition (8-9).

Figure 6 is a comparison between the measured pressure and temperature response of the bed during O_2 injection #3 with both constant and variable permeability model predictions. Note, the oscillations in the experimental pressure trace between 40 and 150 s are caused by piston friction (stick-slip behavior).

Accounting for the variable permeability using the solid mechanics model, improves the results for earlier times. Both the pressure decay and the temperature increase rate are better predicted. However, for later times, there is still substantial disagreement between the results; especially for the temperature response. After about 90 seconds, the temperature curves deviate significantly for both the variable and uniform permeability models. While the experimental result shows that the temperatures continue to increase, both models show that they approach a constant value. These discrepancies are believed to be due to the following:

1. The convective heat exchange model between the reactor and the surroundings might not be applicable for cases with higher internal temperatures and heat generation rates.
2. Morphological changes such as flow channeling and bed sintering could be taking place inside the bed as observed in later experiments done by Shugard *et.al.* (8).

Accounting for bed channeling requires considering a very thin region at the boundary separating the bed from the stainless steel housing (see Figure 1(right)) with a much higher porosity and permeability. At the level of such thin region, the mesh size should be significantly decreased to accurately describe the channeling. Such small mesh size was beyond our computational capabilities and induced instabilities in the numerical schemes used in the model.

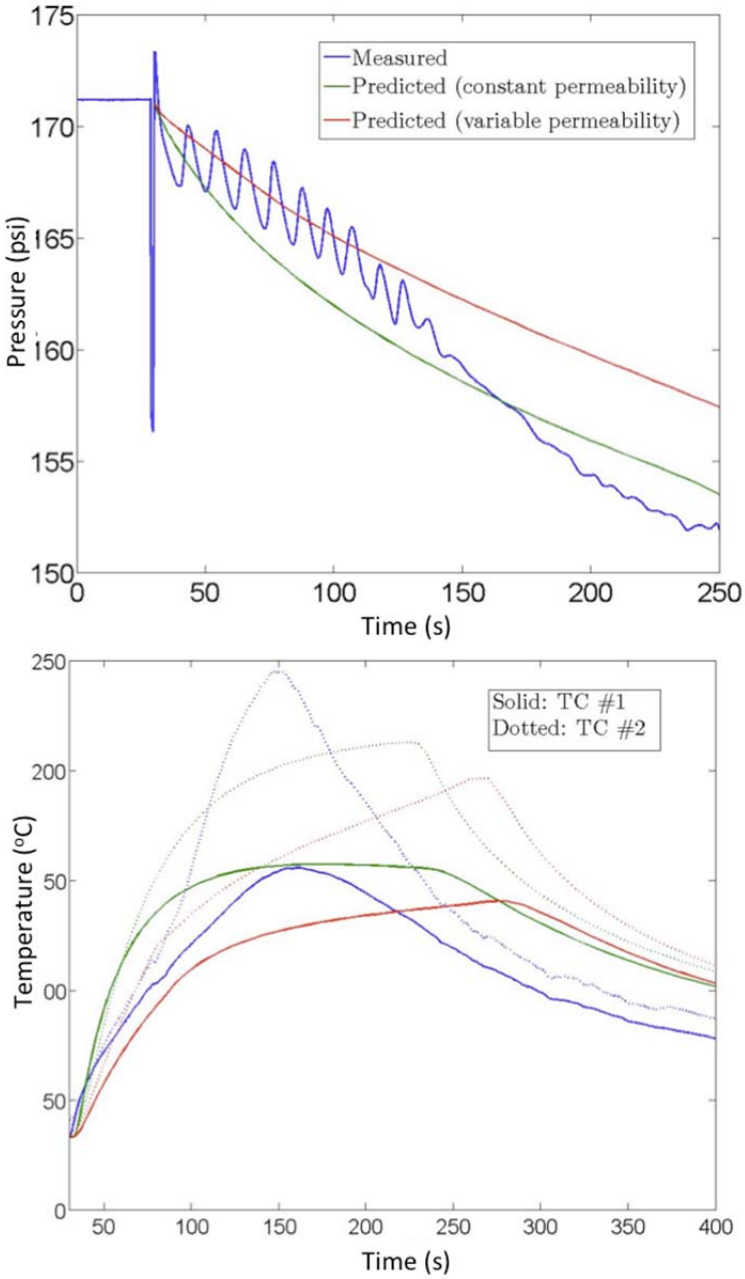

Figure 6: The measured and predicted (top) pressure decay in the O_2 source vessel, (bottom) temperatures at the locations of thermocouples TC #1 and TC #2, as indicated. The predictions were obtained using the constant permeability model of Kanouff *et.al.* (8) and the current variable permeability model for O_2 injection #3.

IMPROVING THE URANIUM HYDRIDE OXIDATION KINETICS PARAMETERS

A pure oxidation experiment is performed of a hydride bed composed of a UD_3-UH_3 mixture through a slow oxygen injection. The variation of the temperature at the outer surface of the bed housing is measured. These measurements provided data for the coupled transport-solid mechanics model in order to optimize for more accurate uranium hydride oxidation kinetics parameters that are more specific to the values of the activation energy and pre-exponential factor.

Pure Oxidation Experiment (Reactor #4)

Reactor #4 is similar in size and design to reactor #1 (described in (8)). The bed is 0.316×0.471 in long and contains 2.78 g of uranium metal. It is instrumented with three 0.032 in sheathed Type-K thermocouples similar to reactor #2 (see (8), Fig. 61). Prior to this oxidation test, it was used for isotope exchange studies described in [8]. In addition, in-situ argon BET surface area measurements were made on this reactor's uranium hydride powder before the oxidation test. The measured powder surface area is 0.80 m^2/g, which is consistent with 0.6 μm diameter solid spherical uranium hydride particles.

This oxygen injection is performed on Reactor #4 simply to fully oxidize the bed for disposal as radioactive waste. However, the test was fully instrumented. The oxygen injection rate was intentionally very low the uranium hydride decomposition rates within the bed were negligible. Consequently, uranium hydride oxidation was the only significant oxygen sink and hydrogen source during this test. Therefore, these test data could be used to better quantify uranium hydride and oxygen reaction rates, without the added complications of hydride decomposition and uranium metal oxidation.

In this test, the piston-driver apparatus (described in (8) and shown below) is used to inject oxygen at a reasonably constant flow rate.

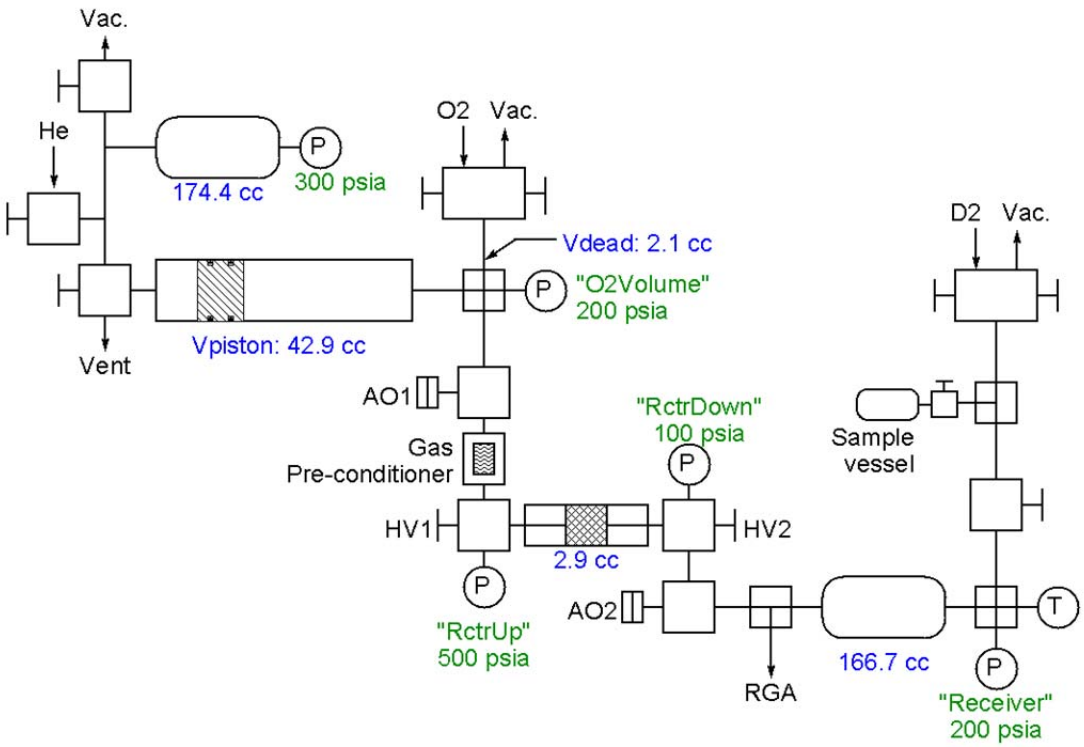

Figure 7: Experimental apparatus used for all uranium hydride reactor experiments. Reproduced from (8).

The oxygen injection rate is limited by throttling the gas using HV1. HV1 is opened very slightly at t=40 s (experiment time). Figure 8 shows measured gas pressures during the test.

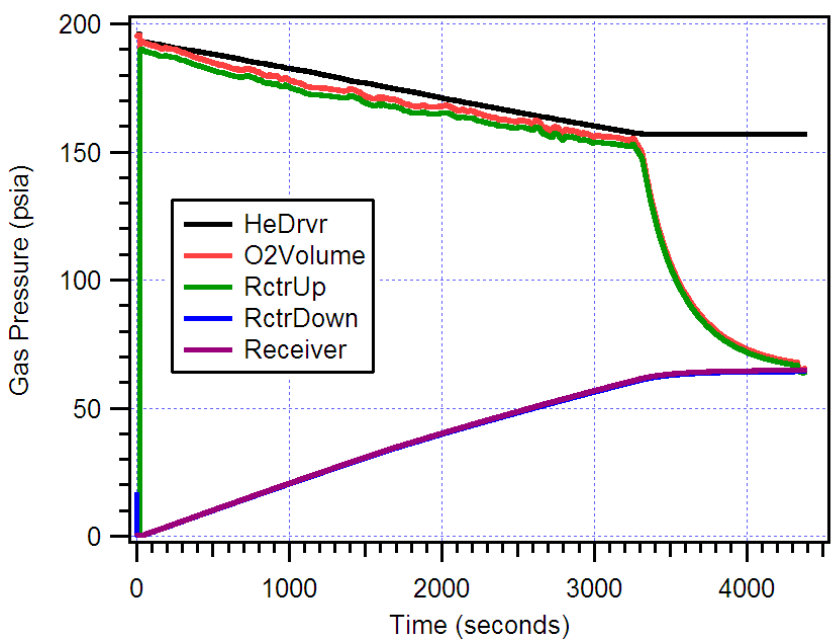

Figure 8: Measured gas pressures during oxygen injection.

Approximately 1.5 times more oxygen is injected than is needed to oxidize the entire bed to U_3O_8. This allows for observation of the oxidation front as it emerged from the bed. The injection rate was low enough that it took about 2200 s (40 min) to oxidize the bed. Since more oxygen is injected than the bed can absorb, pressure equilibrium is not reached until about 4400 s.

Since the RctrUp transducer is upstream of HV1, A pressure measurement on the upstream side of the bed is not available. In addition, because HV1 is an uncharacterized flow restriction, it is difficult to include in our system model. Instead, the O_2 injection rate is computed from the source volume's rate of O_2 gas depletion. The experimentally-derived injection rate and the measured pressure at the reactor outlet are used as boundary conditions in a suitably modified system model. Figure 9 shows the measured O_2 injection rate and a piecewise smooth curve that was used as the model input. The experimental data are noisy because the injection rate is computed using numerical differentiation[1] which greatly amplifies high frequency components in the data record.

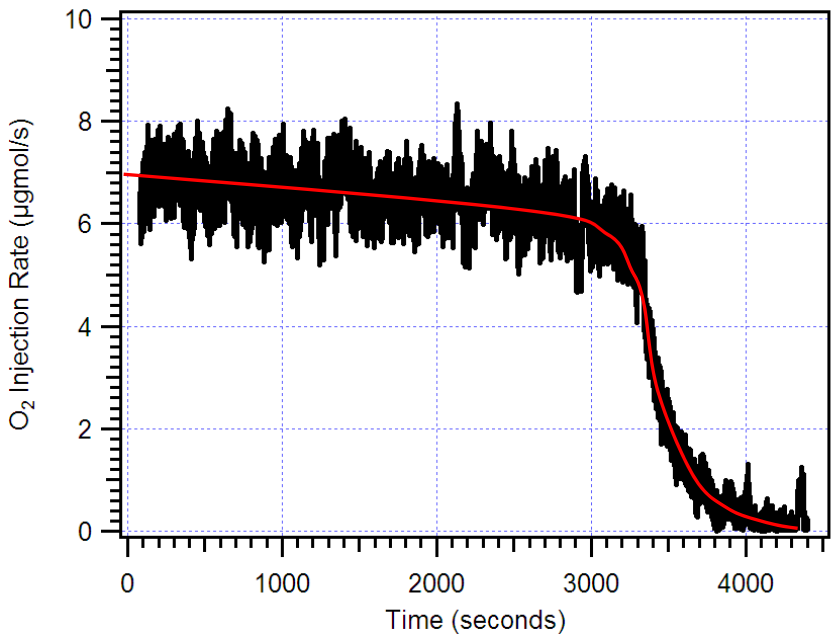

Figure 9: Experimentally measured O_2 injection rate.

Because the original purpose of this test was simply to oxidize the bed for disposal, its initial isotope composition was not a concern. From our analysis of the exchange test data taken prior to this oxygen injection, the bed's composition was 80-85% D and 15-20% H. Since H and D are chemically similar isotopes, it is not expected that this affects the oxidation test results.

Finally, the mass balance results show that only 90% of the bed was oxidized during the test. A post-test bake-out and hydriding test suggests that the other 10% remained as unreacted uranium hydride. We suspect that this 10% did not participate in the oxidation because it was physically

[1] We used a first-order backward differencing scheme with a 40 second time-step.

obstructed by nearby uranium oxide and therefore inaccessible to the flowing oxygen gas. Given the large bed deformations predicted by our model, this does not seem inconceivable.

Even considering these non-idealities, the data generated by this test provide a good set of conditions over which we can test and optimize our uranium hydride oxidation kinetics model.

Fitting the Model to the Experimental Results

The experiment on reactor for is simulated using the coupled transport-solid mechanics model. The O_2 bottle shown in Figure 1 is omitted from the model geometry and the O_2 injection rate at the adjacent boundary is specified. Concurrently, the size the reactor bed and the initial UD_3 concentration is slightly modified to be consistent with this oxidation experiment. The UD_3 oxidation rate is given by:

$$R_{\mathrm{UD_3,ox}} = \beta f_{\mathrm{O_2}} [\mathrm{UD_3}] e^{-E/RT} \tag{11}$$

where f_{O2} is given in (9). β and E are the UD_3 oxidation coefficients that need to be estimated by fitting the temperature response of the bed to measured results. Initially, values are β=4.38 s^{-1} and E=16.63 $kJ.mol^{-1}$. A systematic method is used to minimize the square error between the predicted temperatures and the measured ones. These temperatures are shown in Figure 10. We find the following optimum values for β and E.

$$\begin{aligned} \beta &= 7.13 \text{ s}^{-1} \\ E &= 24.77 \text{ kJ.mol}^{-1} \end{aligned} \tag{12}$$

According to Figure 10, more accurate predictions of the reactor outer wall temperature were obtained using the revised oxidation parameters for the pure oxidation experiment, compared to measured results. It can be concluded that the calibrated oxidation kinetics of UD_3 are slower than the ones previously estimated (8-9).

O_2 injection #2 is simulated again using this revised set of parameters. Based on Figure 11, it is found that major discrepancies between measured and predicted results have decreased relative to the previous case with crude oxidation parameters calibration. Here again, the temperature plots indicated that the oxidation kinetics of UD_3 are slower than the ones previously estimated by Kanouff *et. al.* (8-9).

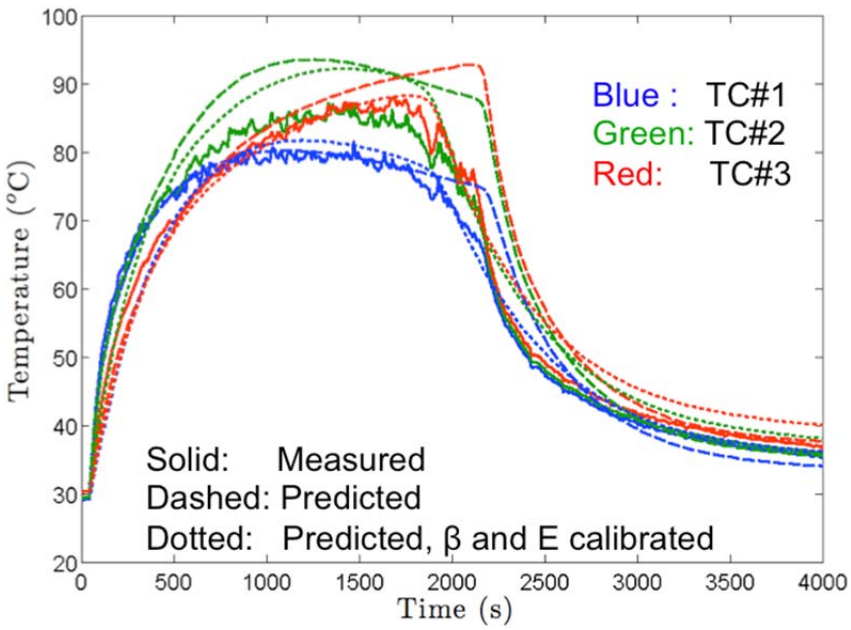

Figure 10: The measured and predicted temperatures at the locations of thermocouples TC #1 TC #2 and TC #3. The predictions were obtained using current variable permeability model for a pure uranium hydride oxidation scenario using the oxidation kinetic coefficients of Kanouff *et.al.* (9) and the values calibrated with experimental measurements, as indicated.

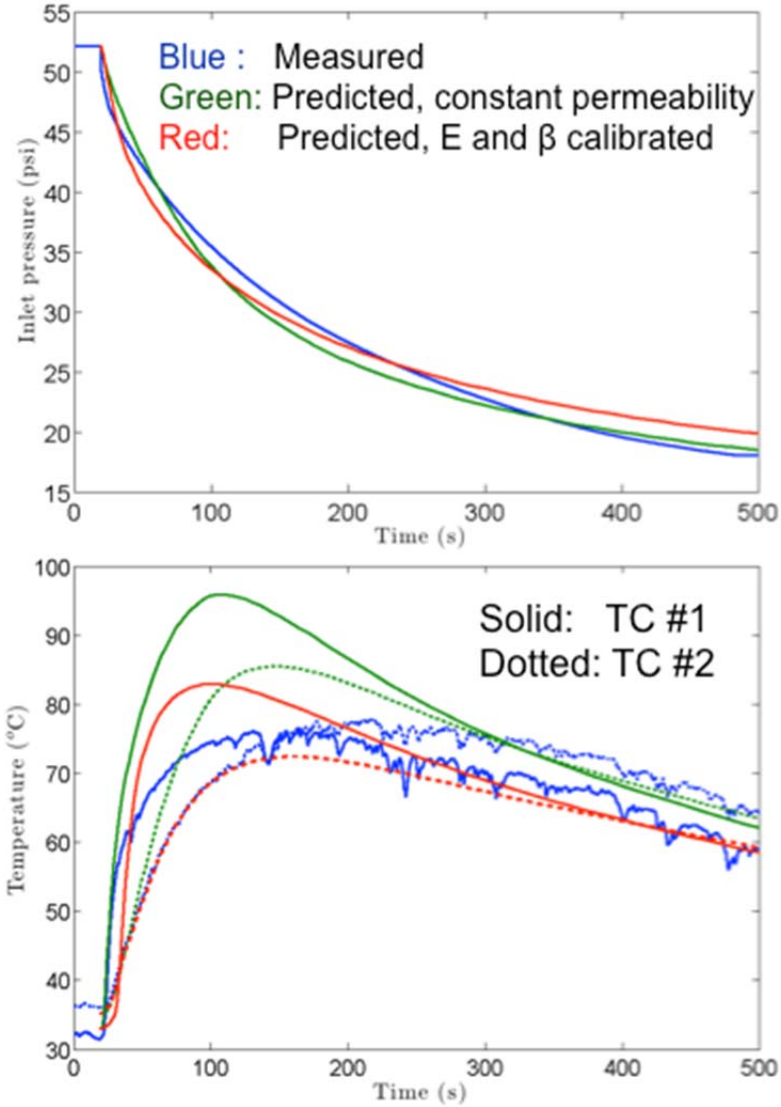

Figure 11: The measured and predicted (top) pressure decay in the O_2 source vessel, (bottom) temperatures at the locations of thermocouples TC #1 and TC #2. The predictions were obtained using current variable permeability model for a pure uranium hydride oxidation scenario using the oxidation kinetic coefficients of Kanouff *et.al.* (9) and the values calibrated with experimental measurements, as indicated.

SUMMARY OF THE GOVERNING EQUATIONS, BOUNDARY CONDITIONS AND NUMERICAL METHODS USED TO MODEL OXIDATION AND DECOMPOSITION IN A URANIUM HYDRIDE BED

In this chapter, the governing equations, geometry, boundary conditions, parameters and numerical methods used to model oxidation and decomposition in a uranium hydride bed are summarized. The mathematical model has already been implemented in a commercial code. We provide recommendations suitable to implement this model on Sandia codes such as ARIA and ADAGIO.

Model Geometry and Mesh

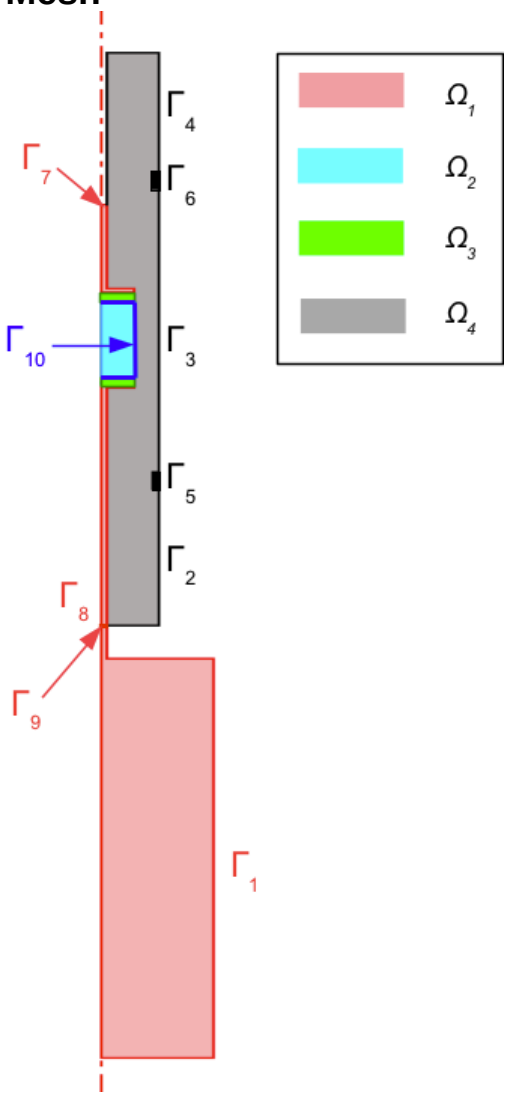

Figure 12: A schematic of the axisymmetric reactor model. The schematic shows the entire model geometry, comprised of subdomains Ω_1, Ω_2, Ω_3 and Ω_4, and boundaries Γ_1, Γ_2 … Γ_{10}.

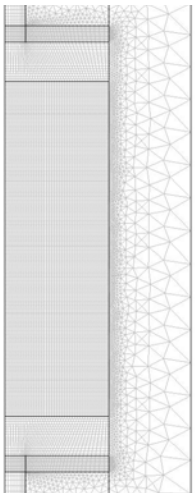

Figure 13: A plot of the recommended mesh inside the bed. The mesh is quadrilateral with a size of 0.1x0.1 mm inside the bed.

Governing Equations and Boundary Conditions

Table 1: Governing Equations and boundary conditions

	Equation	Boundary conditions
Momentum	$\frac{\partial(\rho_{gas}\phi)}{\partial t} - \nabla\cdot\left(\frac{K\rho_{gas}}{\mu}\nabla P\right) = S$ in Ω_1, Ω_2 and Ω_3	$-\hat{\mathbf{n}}.\nabla P = 0$ on Γ_1 and Γ_8 $P = P_{out}(t)$ on Γ_7
Gas Diffusion	$\frac{\partial c}{\partial t} + \nabla\cdot\left(-nD\nabla\left(\frac{c}{n}\right) + c\mathbf{V}\right) = \mathrm{R}_{\mathrm{O}_2}$ in Ω_1, Ω_2 and Ω_3	$-\hat{\mathbf{n}}.\nabla c = 0$ on Γ_1 and Γ_8 $-\hat{\mathbf{n}}.\left[-nD\nabla\left(\frac{c}{n}\right) + c\mathbf{V}\right] = 0$ on Γ_7
Energy	$(\rho c_p)_{bed}\frac{\partial T}{\partial t} + (\rho c_p)_{gas}\mathbf{V}.\nabla T = \nabla.(k_{bed}\nabla T) + Q$ in Ω_2 $(\rho c_p)_{frits}\frac{\partial T}{\partial t} + (\rho c_p)_{gas}\mathbf{V}.\nabla T = \nabla.(k_{frits}\nabla T)$ in Ω_3 $(\rho c_p)_{gas}\frac{\partial T}{\partial t} + (\rho c_p)_{gas}\mathbf{V}.\nabla T = \nabla.(k_{gas}\nabla T)$ in Ω_1 $(\rho c_p)_s\frac{\partial T}{\partial t} = \nabla.(k_s\nabla T)$ in Ω_4	$T = T_l$ on Γ_9 $-\hat{\mathbf{n}}.\nabla T = 0$ on Γ_1, Γ_2, Γ_3, Γ_4, Γ_7 and Γ_8 $-\hat{\mathbf{n}}.[-k_s\nabla T] = h(T_l - T)$ on Γ_5 $-\hat{\mathbf{n}}.[-k_s\nabla T] = h(T_h - T)$ on Γ_6
Solid Species Reaction	$\frac{\partial[\mathrm{UD}_3]}{\partial t} = \mathrm{R}_{\mathrm{UD}_3}$ in Ω_2 $\frac{\partial[\mathrm{U}]}{\partial t} = \mathrm{R}_{\mathrm{U}}$ in Ω_2	$-\hat{\mathbf{n}}.\nabla[\mathrm{UD}_3] = 0$ on Γ_{10} $-\hat{\mathbf{n}}.\nabla[\mathrm{U}] = 0$ on Γ_{10}
Solid Mechanics	$\nabla.[\sigma] = 0$ in Ω_2 $[\varepsilon^e] = \frac{1+\nu}{E}[\sigma] - \frac{\nu}{E}Tr([\sigma])[\mathrm{I}]$ $[\varepsilon] = [\varepsilon^e] + \alpha\Delta T[I] + \sum_{i=\mathrm{U}_3\mathrm{O}_8,\mathrm{U}} \frac{\Delta V_i}{3}x_i[I]$ $[\varepsilon] = \frac{1}{2}\left(\nabla\mathbf{u} + \nabla\mathbf{u}^T\right)$	$-\hat{\mathbf{n}}.\mathbf{u} = 0$ on Γ_{10}

Coupling Relationships

$$\mathbf{V} = -\frac{K}{\mu}\nabla P$$

$$n = \frac{P}{RT}$$

$$n_{bed} = \frac{1}{3}\left(\left[\mathrm{UD_3}\right]^0 + 2\left[\mathrm{UD_3}\right] + 2\left[\mathrm{U}\right]\right)$$

$$\mathrm{R_{O_2}} = -\frac{4}{3}\left(R_{\mathrm{U,ox}} + R_{\mathrm{UD_3,ox}}\right)$$

$$\mathrm{R_{UD_3}} = -R_{\mathrm{UD_3,ox}} - R_{\mathrm{UD_3,dec}}$$

$$\mathrm{R_U} = -R_{\mathrm{U,ox}} - R_{\mathrm{UD_3,dec}}$$

$$R_{\mathrm{UD_{3,dec}}}[\mathrm{s^{-1}}] = \begin{cases} 0 & \text{if } 7.5\times10^{-4}RT(n-c) \geq 10^{9.14-4410/T} \\ 14003[\mathrm{UD_3}]e^{-8630/T} & \text{if } 7.5\times10^{-4}RT(n-c) < 10^{9.14-4410/T} \end{cases}$$

$$R_{\mathrm{UD_3,ox}}[\mathrm{s^{-1}}] = 7.13 f_{\mathrm{O_2}}[\mathrm{UD_3}]e^{-24.77[\mathrm{kJ.mol^{-1}}]/RT}$$

$$R_{\mathrm{U,ox}}[\mathrm{s^{-1}}] = 4.38 f_{\mathrm{O_2}}[\mathrm{U}]e^{-16.63[\mathrm{kJ.mol^{-1}}]/RT}$$

Table 2: Thermophysical properties of the species present in the model

	O_2	D_2	UD_3	U	U_3O_8
M (g.mol^{-1})	32	4	244	238	842
ρ (g.cm^{-3})	$cM_{\mathrm{O_2}}$	$\rho - cM_{\mathrm{O_2}}$	10.95	19.1	8.38
C_p (J.mol^{-1}.K^{-1})	1.664+10.69 $\log_{10}$ (T)	7.07+7.9×10^{-4}T(°C)	49.3	27.7	238
k (W.cm^{-1}.K^{-1})	$1.63\times10^{-4}\left(\frac{T}{273}\right)^{0.73}$	$1.63\times10^{-4}\left(\frac{T}{273}\right)^{0.73}$	0.01	0.01[27+0.0214(T-300)]	0.000838
μ (g.cm^{-1}.s^{-1})	1.92×10^{-4}	1.192×10^{-4}	-	-	-
ϕ_0	-	-	0.605	0.776	0.393
ΔV	-	-	-	-0.432	0.536

Table 3: Thermomechanical properties of the solid species present in the model

	UD_3	U	U_3O_8
E (barye)	$2.15\text{x}10^{12}[1-0.00016\ T(^{o}\text{C})]$	$10^{12}(2.4-0.00063T(^{o}\text{C})-9\text{x}10^{-7}\ T(^{o}\text{C})^2)$	$2.15\text{x}10^{12}[1-0.00016\ T(^{o}\text{C})]$
ν	$0.32-0.34\ \phi$	$0.11+0.0001T(^{o}\text{C})+1.3\text{x}10^{-7}\ T(^{o}\text{C})^2$	$0.32-0.34\ \phi$
α (K^{-1})	$1.37\text{x}10^{-5}$ if $T<400\ ^{o}\text{C}$ $1.66\text{x}10^{-5}$ if $T\geq 400\ ^{o}\text{C}$	$1.39\text{x}10^{-5}$	$6\text{x}10^{-6}T(^{o}\text{C})+2\text{x}10^{-9}T(^{o}\text{C})^2+1.7\text{x}10^{-19}T(^{o}\text{C})^3$

Table 4. Physical properties of the species present in the model

	Ω_1	Ω_2	Ω_3	Ω_4
k ($W.cm^{-1}.K^{-1}$)	$1.63\times10^{-4}\left(\frac{T}{273}\right)^{0.73}$	$\frac{1}{\phi n_{bed}}\sum_{UD_3,U,U_3O_8} k_i\phi_{0,i}[i]$	0.1	0.15
c_p ($J.g^{-1}.K^{-1}$)	$\frac{1}{\rho}\sum_{i=O_2,D_2}\rho_i c_{p,i}$	$\frac{\sum_{i=UD_3,U,U_3O_8} C_{p,i}[i]}{\sum_{i=UD_3,U,U_3O_8} M_i[i]}$	0.5	0.5
μ ($g.cm^{-1}.s^{-1}$)	$\frac{1}{n}\sum_{i=O_2,D_2}\mu_i[i]\left(\frac{T}{273}\right)^{0.73}$	$\frac{1}{n}\sum_{i=O_2,D_2}\mu_i[i]\left(\frac{T}{273}\right)^{0.73}$	$\frac{1}{n}\sum_{i=O_2,D_2}\mu_i[i]\left(\frac{T}{273}\right)^{0.73}$	-
ρ ($g.cm^{-3}$)	$cM_{O_2}+(n-c)M_{D_2}$	$\sum_{i=UD_3,U,U_3O_8} M_i[i]$	6.26	7.92
κ (cm^2)	10^{-3}	$\frac{\phi d_p^2}{\tau^2}\left(\frac{1}{32}+\frac{5}{12}\frac{RT}{\pi d_p\sqrt{2}N_A P d_{O_2}^2}\right)$	$\frac{\phi d_{p,f}^2}{\tau_f^2}\left(\frac{1}{32}+\frac{5}{12}\frac{RT}{\pi d_{p,f}\sqrt{2}N_A P d_{O_2}^2}\right)$	-
D ($cm^2.s^{-1}$)	$\frac{1.25}{P(\text{atm})}\left(\frac{T}{400}\right)^{1.404}$	$\frac{1.25\phi}{P(\text{atm})}\left(\frac{T}{400}\right)^{1.404}$	$\frac{1.25\phi_f}{P(\text{atm})}\left(\frac{T}{400}\right)^{1.404}$	-
φ	-	$1-\frac{(1-\phi_0)\left(1+\frac{1}{n_{bed}}\sum_{i=U_3O_8,U}\Delta V_i[i]\right)}{1+e}$	0.3	-

Recommendation for ARIA Developers

The PDEs involved in the uranium hydride oxidation and decomposition transport model are nonlinear and highly coupled. Several considerations should be taken by the code developers in order to fully and accurately implement the model on ARIA. These considerations include:

- The diffusion term in the gas diffusion equation accounts for the variability of the gas density in the simulation domain. It is therefore written in its nonlinear form: $\frac{\partial c}{\partial t} + \nabla \cdot \left(-nD\nabla\left(\frac{c}{n}\right) + c\mathbf{V} \right) = R_{O_2}$

  The diffusion term requires more development on ARIA to be properly accounted for.
- The sub-models coupling equations and nonlinear materials properties listed above should be carefully programmed as user subroutines.
- The partial derivatives of the coupling equations and nonlinear materials properties should be properly computed as a function of the solved variables to compute the Jacobian matrices.
- ADAGIO needs some more development to account for temperature and composition dependent expansion coefficients.
- Both ARIA and ADAGIO might need more development to properly couple the solid mechanics and transport models in this application.
- ADAGIO requires a fully Lagrangian solution scheme of the solid mechanics equations in order to account for the large deformation in the bed.

CONCLUSIONS

This report describes the model development of an advanced hydrogen storage system. The results show that by coupling the solid mechanical and transport models, the agreement between simulated and measured bed response are improved. Implementing the new set of uranium hydride oxidation parameters in the coupled transport-solid mechanics model shows that the agreement between the predicted and measured results is further improved.

REFERENCES

1. C.C. Bowman and V.A. Vis. Tritium handling facility at KMS fusion inc. J. Vac. Sci. Tech. A: Vacuum, Surfaces, and Films, 8(3):2890, 1990.
2. L.K. Heung. Tritium transport vessel using depleted uranium. *Fusion. Tech.*, 28(3):1385, 1995.
3. T. Hayashi et.al. Safe handling experience of a tritium storage bed. *Fusion. Eng.Des.*, 83:1429, 2008.
4. T.C. Totemeier. Characterization of uranium corrosion products involved in a uranium hydride pyrophoric event. J. Nucl. Mat., 278(2-3):301, 2000.
5. F. Le Guyadec *et.al.* Pyrophoric behaviour of uranium hydride and uranium powders. *J. Nucl. Mat.*, 396:294, 2010.
6. G.R. Longhurst. Pyrophoricity of tritium-storage bed materials. *Fusion. Tech.*, 14:750, 1988.
7. G.L. Powell. Reaction of oxygen with uranium hydride. In Advanced Materials for Energy Conversion, Chandra, 2004.
8. A.D. Shugard, G.M. Buffleben, M.P. Kanouff, S.C. James, D.B. Robinson, B.E. Mills, P.E. Gharagozloo, and P. Van Blarigan. Rapid hydrogen gas generation using reactive thermal decomposition of uranium hydride. Report SAND2011-6939, Sandia National Laboratories, 2011.
9. M.P. Kanouff, P.E. Gharagozloo, M. Salloum, A.D. Shugard "A Multiphysics Numerical Model of Oxidation and Decomposition in a Uranium Hydride Bed" Chem. Eng. Sci. (in press).
10. J.B. Young and B. Todd. Modeling of multi-component gas flows in capillaries and porous solids. Int. J. Heat. Mass. Trans., 48:5338, 2005.
11. S.L. Robinson and G.J. Thomas. Uranium Hydride Formation and Properties: A Review with Commentary on Handling and Disposition. SAND96-8206. Sandia National Labs. (1996).
12. E.S. Fischer "Temperature dependence of the elastic moduli in alpha uranium single crystals, part IV (298 K to 923 K)" J. Nucl. Mat., 18:39-54, 1966.
13. T.R.G. Kutty, K.N. Chandrasekharan, J.P. Panakkal and J.K. Ghosh. "Fracture toughness and fracture surface energy of sintered uranium dioxide fuel pellets" J. Mat. Sci. Lett., 6:260-262, 1987.
14. M.O. Marlow "High temperature isothermal elastic moduli of UO_2" J. Nucl. Mat., 33:242-244, 1969.C
15. Y. Wu, O.M. Ruddy, A.C. Bentham, B.C. Hancock, S.M. Best, J.A. Elliott. Modelling the mechanical behaviour of pharmaceutical powders during compaction. Powder Technology., 152:107-117, 2005.
16. F.D. Manchester and A. San-Martin "The H-U (Hydrogen-Uranium) System" J. Phase. Equil., 16(3):263-275, 1995.
17. F.A. Halden, H. C. Wohlers and R.H. Reinhart. "Thermal expansion of uranium dioxide" United States Atomic Energy Commission, Metallurgy and Materials Branch, Washington D.C., April 1959.
18. Comsol Multiphysics 3.5a, Solid Mechanics Module User's Manual, Comsol Inc., 2008.

19. R.D. Kosalinski, A.D. Shugard, C.R. Tewell, D.F. Cowgill. Uranium for Hydrogen Storage Applications: A Material Science Perspective. Report SAND2010-5195, Sandia National Laboratories, 2010.
20. S.M. Thein, P.J. Bereolos. Thermal Stabilization of $233UO_2$, $233UO_3$ and $233U_3O_8$. Report ORNL/TM-2000/82, Oak Ridge National Laboratories, July 2000.
21. Touloukian, Y.S., ed., 1967. Thermophysical Properties of High Temperature Materials, Vol. 4: Oxides and Their Solutions and Mixtures, Part 1: Simple Oxygen Compounds and Their Mixtures. MacMillan Company, New York.
22. C.W. Nan, R. Birringer. Effective thermal conductivity of particulate composites with interfacial thermal resistance. J. Appl. Phys., 81:10, 1997.

DISTRIBUTION

(all copies electronic)

1	MS0828	Ryan B. Bond	1541
1	MS0899	Technical Library	9536
1	MS9035	Paul A. Spence	8254
1	MS9042	Michael L. Chiesa	8259
1	MS9042	Christopher D. Moen	8256
1	MS9158	Maher Salloum	8961
1	MS9161	George M. Buffleben	8651
1	MS9291	David Robinson	8651
1	MS9403	Bernice E. Mills	8131
1	MS9409	Gregory J. Wagner	8365
1	MS9409	Patricia E. Gharagozloo	8365
2	MS9960	Technical Library – CA	8944
1	MS9661	Andrew D Shugard	8254

Sandia National Laboratories